

Effects of Cu and Co additions on the crystallization and magnetic properties of FeNbB alloy

Wan-Qiu Yu(于万秋), Bo Tian(田博), Ping-Li Zhang(张平丽), Jia-Hui Wang(王佳慧), and Zhong Hua(华中)
Citation: Chin. Phys. B, 2023, 32 (**8**): 088102. DOI: 10.1088/1674-1056/acd525
Journal homepage: http://cpb.iphy.ac.cn; http://iopscience.iop.org/cpb

What follows is a list of articles you may be interested in

Phase-field study of spinodal decomposition under effect of grain boundary

Ying-Yuan Deng(邓英远), Can Guo(郭灿), Jin-Cheng Wang(王锦程), Qian Liu(刘倩), Yu-Ping Zhao(赵玉平), and Qing Yang(杨卿)
Chin. Phys. B, 2021, 30 (**8**): 088101. DOI: 10.1088/1674-1056/abea9b

Effects of Nb and Mo additions on thermal behavior, microstructure and magnetic property of FeCoZrBGe alloy

Yaming Sun(孙亚明), Zhiqun Wang(王志群), Shi-Chong Xu(徐仕翀), and Zhong Hua(华中)
Chin. Phys. B, 2021, 30 (**3**): 038103. DOI: 10.1088/1674-1056/abc7a8

High temperature strain glass in Ti-Au and Ti-Pt based shape memory alloys

Shuai Ren(任帅), Chang Liu(刘畅), and Wei-Hua Wang(汪卫华)
Chin. Phys. B, 2021, 30 (**1**): 018101. DOI: 10.1088/1674-1056/abc54a

Dependence of mechanical properties on the site occupancy of ternary alloying elements in γ'-Ni_3Al: *Ab initio* description for shear and tensile deformation

Minru Wen(文敏儒), Xing Xie(谢兴), Huafeng Dong(董华锋), Fugen Wu(吴福根), Chong-Yu Wang(王崇愚)
Chin. Phys. B, 2020, 29 (**7**): 078103. DOI: 10.1088/1674-1056/ab8a38

Atomically flat surface preparation for surface-sensitive technologies

Cen-Yao Tang(唐岑瑶), Zhi-Cheng Rao(饶志成), Qian-Qian Yuan(袁茜茜), Shang-Jie Tian(田尚杰), Hang Li(李航), Yao-Bo Huang(黄耀波), He-Chang Lei(雷和畅), Shao-Chun Li(李绍春), Tian Qian(钱天), Yu-Jie Sun(孙煜杰), Hong Ding(丁洪)
Chin. Phys. B, 2020, 29 (**2**): 028101. DOI: 10.1088/1674-1056/ab6586

Effects of Cu and Co additions on the crystallization and magnetic properties of FeNbB alloy

Wan-Qiu Yu(于万秋)[†], Bo Tian(田博), Ping-Li Zhang(张平丽), Jia-Hui Wang(王佳慧), and Zhong Hua(华中)

College of Physics, Jilin Normal University, Siping 136000, *China*

(Received 7 March 2023; revised manuscript received 23 April 2023; accepted manuscript online 12 May 2023)

The nanocrystalline-forming element Cu and magnetic element Co are commonly used as additive elements to tune the structure and improve the properties of alloys. In this study, four kinds of amorphous alloys, $Fe_{72}Nb_{12}B_{16}$, $Fe_{72}Nb_{12}B_{15}Cu_1$, $Fe_{36}Co_{36}Nb_{12}B_{16}$, and $Fe_{36}Co_{36}Nb_{12}B_{15}Cu_1$, were prepared by melt-spinning and annealed at various temperatures to investigate the effects of Cu and Co additions, individually and in combination, on the crystallization and magnetic properties of $Fe_{72}Nb_{12}B_{16}$ alloy. The four kinds of alloys exhibited different crystallization behaviors with different primary crystallization phases observed. For the $Fe_{72}Nb_{12}B_{16}$ alloy, only the α-Mn-type metastable phase formed after annealing. The addition of 1 at.% Cu and 36 at.% Co led to the observation of the α-Mn-type and β-Mn-type metastable phases, respectively, and a reduction in the crystallization volume fraction in the metastable phase. The $Fe_{36}Co_{36}Nb_{12}B_{15}Cu_1$ alloy only exhibited α-Fe(Co) phase as a primary phase, and the addition of both Cu and Co completely inhibited the precipitation of the metastable phase. Cu clusters were found in energy dispersive spectroscopy elemental maps. Compared with other alloys, $Fe_{36}Co_{36}Nb_{12}B_{15}Cu_1$ alloy with both Cu and Co exhibited a lower coercivity (H_c) below 973 K.

Keywords: alloys, nanocrystalline, Cu addition, Co addition

PACS: 81.07.–b **DOI:** 10.1088/1674-1056/acd525

1. Introduction

Fe-based nanocrystalline soft magnetic alloys have attracted considerable attention, as they exhibit better synthetic soft magnetic properties than that of traditional soft magnetic materials and display excellent energy-saving and environmental protection characteristics.[1–7] The composition design and microstructure control of Fe-based nanocrystalline soft magnetic alloys are important.

Fe-based nanocrystalline soft magnetic alloys can be divided into five main categories: FeCuNbSiB (Finemet),[8] FeMB(Cu) (M = Zr, Nb, Hf; Nanoperm),[9] FeCoMB(Cu) (M = Zr, Nb, Hf; Hitperm),[10] FeSiBPCu (Nanomet),[11] and FeSiBPCCu (HBNAs).[12] For these five types of alloys, the alloy elements are typically divided into three categories according to their roles in the alloys: magnetic elements (Fe, Co, and Ni), amorphous-forming elements (such as B, Si, P, and C), and nanocrystalline-forming elements (such as Cu, Ag, and Au). The nanocrystalline-forming element Cu and magnetic element Co are common and important additive elements that are used to tune the structure and improve the properties of alloys.

The influence of Cu addition on the microstructures and properties of Fe-based alloys has been widely investigated.[13–21] Cu clustering forms prior to the onset of the primary crystallization reaction and serves as a heterogeneous nucleation site for α-Fe for many Fe-based alloys.[19] For most Fe-based alloys, 1 at.% Cu can completely play the role of heterogeneous nucleation.

Replacing Fe with Co in Fe-based soft magnetic alloys can affect the crystallization processes,[22] improve the high temperature soft magnetic properties[10] and saturation magnetization,[23] increase the Curie temperature,[24] and improve the plastic deformation ability of the Fe-based alloy.[25] Research on the effects of Co substitution of Fe on the structure and properties of such alloys is of considerable scientific interest.

Hitperm series alloys FeCoMB(Cu) (M = Zr, Nb, Hf) can be seen as the development of partially substituting Co for Fe in Nanoperm FeMB(Cu) (M = Zr, Nb, Hf) alloys. However, the addition effect of Cu on the two kinds of alloys is different. For FeZrB alloys without Co,[26] the substitution of 1 at.% Cu for Fe in both low- and high-boron-content alloys has significant effects on the microstructure and magnetic properties. For FeCoZrBCu alloy with high Co content,[20] 1 at.% Cu addition is unnecessary (Hitperm composition $Fe_{44}Co_{44}Zr_7B_4Cu_1$ alloy). It is thus clear that not all Cu undergoes heterogeneous nucleation. In this study, $Fe_{72}Nb_{12}B_{16}$, $Fe_{72}Nb_{12}B_{15}Cu_1$, $Fe_{36}Co_{36}Nb_{12}B_{16}$, and $Fe_{36}Co_{36}Nb_{12}B_{15}Cu_1$ amorphous and nanocrystalline alloys are prepared. The effects of Cu and Co addition, individually and in combination, on the crystallization and magnetic properties of the $Fe_{72}Nb_{12}B_{16}$ alloy are investigated. The research in this paper will further supplement the research on the effect of 1 at.% Cu addition on the FeNbB

[†]Corresponding author. E-mail: yuwanqiu2004@126.com

© 2023 Chinese Physical Society and IOP Publishing Ltd

and FeCoNbB alloys.

2. Experiment

Ingots with the nominal compositions $Fe_{72}Nb_{12}B_{16}$, $Fe_{72}Nb_{12}B_{15}Cu_1$, $Fe_{36}Co_{36}Nb_{12}B_{16}$, and $Fe_{36}Co_{36}Nb_{12}B_{15}Cu_1$ were produced by arc melting mixtures of high-purity Fe (99.98 wt%), Co (99.97 wt%), Nb (99.9 wt%), B (99.999 wt%), and Cu (99.99 wt%) in a high Ar gas atmosphere. To ensure the homogeneity of the compositions, the ingots were remelted four times with magnetic stirring. The as-quenched ribbons with thicknesses of approximately 30 μm and widths of approximately 1 cm were prepared via a melt-spinning method with a copper-wheel rate of 38 m/s. These as-quenched ribbons were annealed at 823 K, 848 K, 873 K, 923 K, 973 K, and 1023 K for 40 min under vacuum.

Differential scanning calorimetry (DSC) traces of amorphous alloys were investigated by a simultaneous thermal analyzer (STA, STA 449F5). The microstructures of the alloys were characterized via x-ray diffraction (XRD, D/max 2500/PC) with Cu-$K\alpha$ radiation and transmission electron microscopy (TEM). The grain size was determined using the Jade 5.0 software. TEM imaging and energy dispersive spectroscopy (EDS) were performed using an FEI Talos F200X. The grain size distribution was obtained using a nano measurer. Coercivity (H_c) was determined using a vibrating sample magnetometer (VSM, Lake Shore M7407).

3. Results and discussion

XRD patterns of the $Fe_{72}Nb_{12}B_{16}$, $Fe_{72}Nb_{12}B_{15}Cu_1$, $Fe_{36}Co_{36}Nb_{12}B_{16}$, and $Fe_{36}Co_{36}Nb_{12}B_{15}Cu_1$ alloys as-quenched are shown in Fig. 1(a). No crystalline peaks can be observed in the XRD patterns of the as-quenched alloys, implying that they are all in the amorphous state. The corresponding DSC traces are shown in Fig. 1(b). A heat treatment interval of 25 K was set at a lower temperature to observe the initial crystallization phase more carefully. Within the range of 873 K–1023 K, heat treatment was carried out every 50 K to observe and compare the crystalline phases of different alloys at the same temperature.

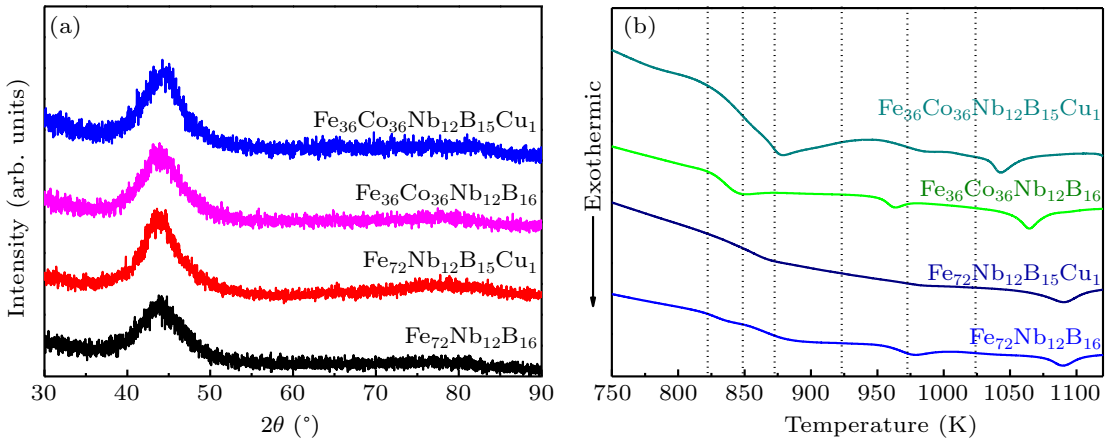


Fig. 1. (a) XRD patterns and (b) DSC traces of the $Fe_{72}Nb_{12}B_{16}$, $Fe_{72}Nb_{12}B_{15}Cu_1$, $Fe_{36}Co_{36}Nb_{12}B_{16}$, and $Fe_{36}Co_{36}Nb_{12}B_{15}Cu_1$ alloys as-quenched.

XRD patterns of the $Fe_{72}Nb_{12}B_{16}$, $Fe_{72}Nb_{12}B_{15}Cu_1$, $Fe_{36}Co_{36}Nb_{12}B_{16}$, and $Fe_{36}Co_{36}Nb_{12}B_{15}Cu_1$ alloys after annealing at various temperatures are shown in Fig. 2. With increase in the annealing temperature, some crystalline phases precipitate from the amorphous matrix.

The primary crystallization phases of the four kinds of alloys are different. The fitting spectra of four kinds of alloys annealed at 848 K are shown in Fig. 3. For the $Fe_{72}Nb_{12}B_{16}$ alloy, only the α-Mn-type structure phase precipitates as the primary phase. For the $Fe_{72}Nb_{12}B_{15}Cu_1$ alloy, two types of crystalline phases are observed: the α-Mn-type structure phase and the α-Fe crystalline phase. For the $Fe_{36}Co_{36}Nb_{12}B_{16}$ amorphous alloy, the crystalline phases consist of small amounts of the β-Mn-type structure phase and large proportions of the α-Fe(Co) phase. The α-Mn-type structure and β-Mn-type structure phases are also designated as χ-phase and π-phase, respectively.[7] The compositions of α-Mn-type[15,27–29] and β-Mn-type[6,30] structure phases do not include Mn and are common metastable phases in the early crystallization stage of Fe-based amorphous alloys. They possess structures relate to tetrahedrally close-packed (TCP) structures, comprising mainly coordination Frank–Kasper polyhedra (= 12, 14, 15, 16).[7] The crystallization volume fraction of the metastable phase is reduced at the primary crystallization stage when 1 at.% Cu and 36 at.% Co are added, respectively. For the FeNbB(Cu) alloys without Co, it is easier to generate the α-Mn-type phases, while for the FeCoNbB alloys with high Co content, it is easier to generate the β-Mn-type phase. For $Fe_{36}Co_{36}Nb_{12}B_{15}Cu_1$ alloy, the primary crystallization phase is only α-Fe(Co) phase.

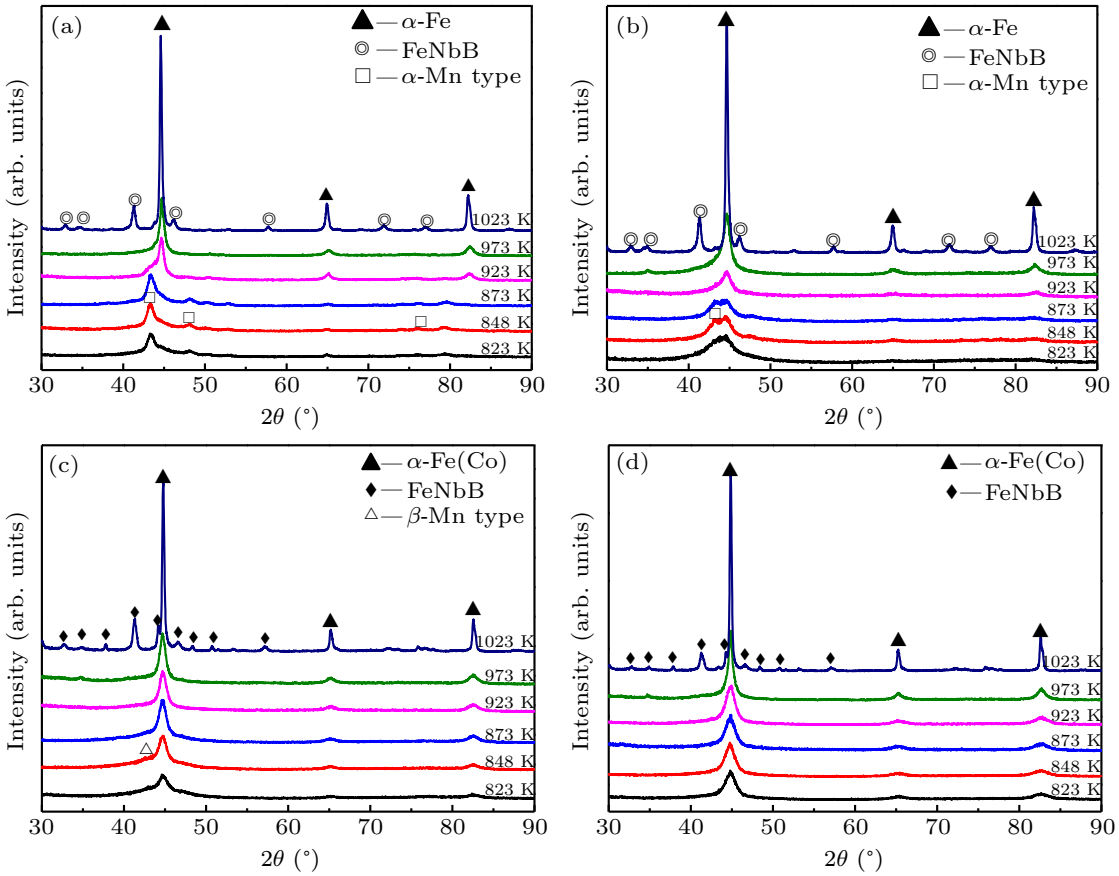


Fig. 2. XRD patterns of (a) $Fe_{72}Nb_{12}B_{16}$, (b) $Fe_{72}Nb_{12}B_{15}Cu_1$, (c) $Fe_{36}Co_{36}Nb_{12}B_{16}$, and (d) $Fe_{36}Co_{36}Nb_{12}B_{15}Cu_1$ alloys after annealing at various temperatures.

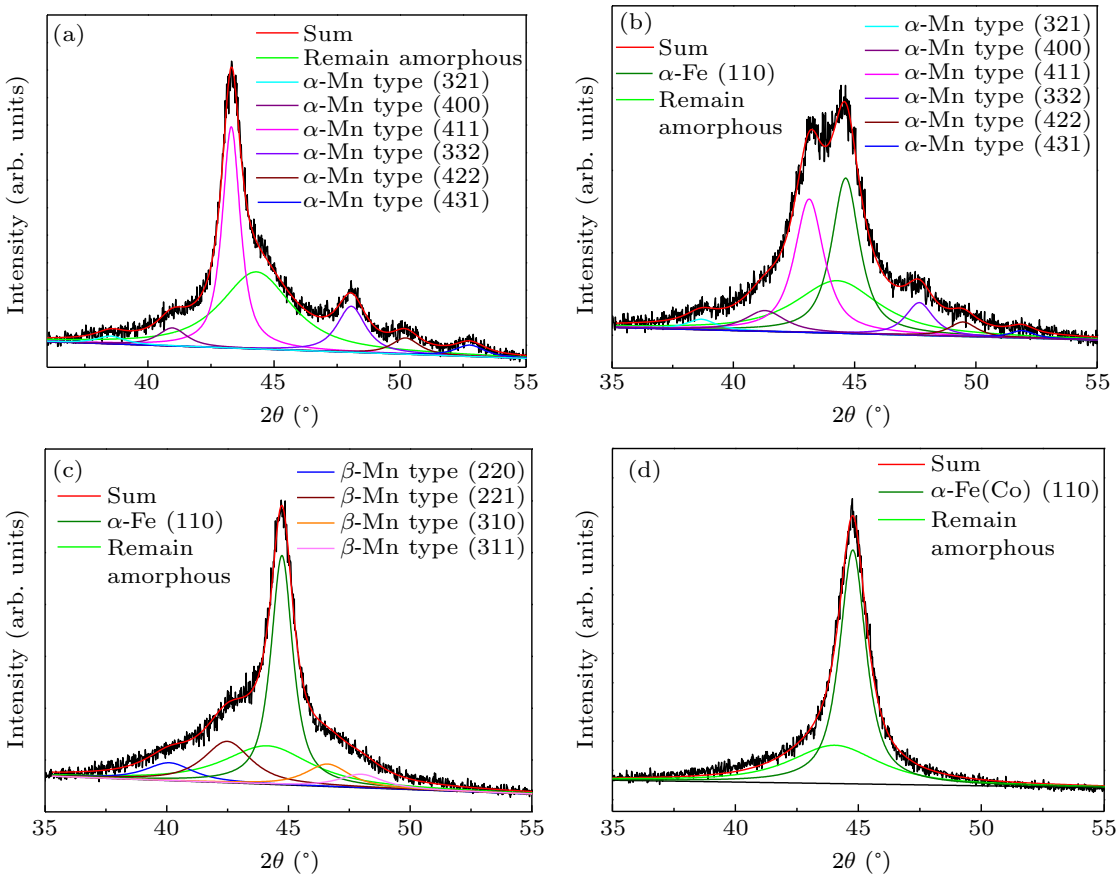


Fig. 3. Fitting spectra of (a) $Fe_{72}Nb_{12}B_{16}$, (b) $Fe_{72}Nb_{12}B_{15}Cu_1$, (c) $Fe_{36}Co_{36}Nb_{12}B_{16}$, and (d) $Fe_{36}Co_{36}Nb_{12}B_{15}Cu_1$ amorphous alloys annealed at 848 K.

With higher annealing temperatures, the volume fraction of the metastable phase decreases and transforms into an α-Fe solid solution phase for the $Fe_{72}Nb_{12}B_{16}$, $Fe_{72}Nb_{12}B_{15}Cu_1$, and $Fe_{36}Co_{36}Nb_{12}B_{16}$ alloys. With the increase of annealing temperature, the crystallization volume fraction (V_{cry}) of crystallization phases gradually increases. When the annealing temperature is 973 K, no metastable phases can be observed and the grain size [α-Fe/α-Fe(Co)] of the three kinds of alloys is 14.4 nm, 7.9 nm, and 9.8 nm, respectively. For $Fe_{36}Co_{36}Nb_{12}B_{15}Cu_1$ alloy, only α-Fe(Co) phase can be observed below 973 K. With the increase of annealing temperature, the crystallization volume fraction (V_{cry}) and grain size (D) of α-Fe(Co) phase gradually increase. The grain size of the alloy annealed at 823 K, 848 K, 873 K, 923 K, 973 K, and 1023 K is 6.1 nm, 6.3 nm, 6.9 nm, 7.8 nm, 10.2 nm, and 39.4 nm, respectively. After annealing at 1023 K, a large number of compounds form for the four kinds of alloys.

Transmission electron microscopy (TEM) is one of the most important testing methods for observing the microstructure of materials.[31,32] Figure 4 shows the TEM images, the corresponding selected area electron diffraction (SAED) patterns, the high-resolution transmission electron microscope (HRTEM) images and the corresponding fast Fourier transforms (FFTs) patterns of $Fe_{72}Nb_{12}B_{16}$ (a, a′), $Fe_{72}Nb_{12}B_{15}Cu_1$ (b, b′), $Fe_{36}Co_{36}Nb_{12}B_{16}$ (c, c′), and $Fe_{36}Co_{36}Nb_{12}B_{15}Cu_1$ (d, d′) alloys annealed at 848 K. The TEM images of the alloys show that the nanocrystals embedded in the residual amorphous matrix distribute uniformly and display almost no grain agglomeration. For the $Fe_{72}Nb_{12}B_{16}$ alloy, only the α-Mn type phase is confirmed by the diffraction rings [Fig. 4(a)]. The high-resolution image is shown in Fig. 4(a′). The corresponding diffraction pattern after FFT conversion (upper right corner) shows that the grain is an α-Mn phase grain and that the crystal band axis is [311]. The SAED analyses confirm that the metastable phases can be observed in the images for the $Fe_{72}Nb_{12}B_{15}Cu_1$ [Fig. 4(b)] and $Fe_{36}Co_{36}Nb_{12}B_{16}$ alloys [Fig. 4(c)]. The HRTEM image of $Fe_{72}Nb_{12}B_{15}Cu_1$ alloy and diffraction pattern after FFT conversion [Fig. 4(b′)] indicates that the large grain is an α-Mn-type phase grain and that the crystal band axis is [311]. The HRTEM image of $Fe_{36}Co_{36}Nb_{12}B_{16}$ alloy and diffraction pattern after FFT conversion [Fig. 4(c′)] indicates that the large grain is a β-Mn-type phase grain with an irregular shape and that the crystal band axis is [331]. For $Fe_{36}Co_{36}Nb_{12}B_{15}Cu_1$ alloy, TEM results further reveal that no other phase can be observed than α-Fe(Co). The high-resolution image and the corresponding diffraction pattern after FFT conversion [Fig. 4(d′)] indicate that the grain is an α-Fe(Co) phase grain and that the crystal band axis is [111].

According to Figs. 4(a)–4(d), 200 grains are measured from every image. The grain size distributions of the four kinds of alloys annealed at 848 K are provided in Figs. 5(a)–5(d). The grain size distributions are fitted by a log-normal function.[33] The mean grain sizes are shown in the upper right corner. The addition of 1 at.% Cu decreases the grain size and the addition of 36 at.% Co has little impact. The grain size of the $Fe_{36}Co_{36}Nb_{12}B_{15}Cu_1$ alloy with both Cu and Co is remarkably refined.

Figure 6 shows the TEM morphology and the corresponding EDS elemental maps of the $Fe_{36}Co_{36}Nb_{12}B_{15}Cu_1$ alloy annealed at 848 K. The EDS elemental maps show that the distribution of Cu is different from that of the others elements. The distribution of Cu is inhomogeneous and there are Cu-rich areas, which can be considered as Cu clusters. According to the previous study, the Cu clusters may serve as heterogeneous nucleation sites for α-Fe(Co).[19]

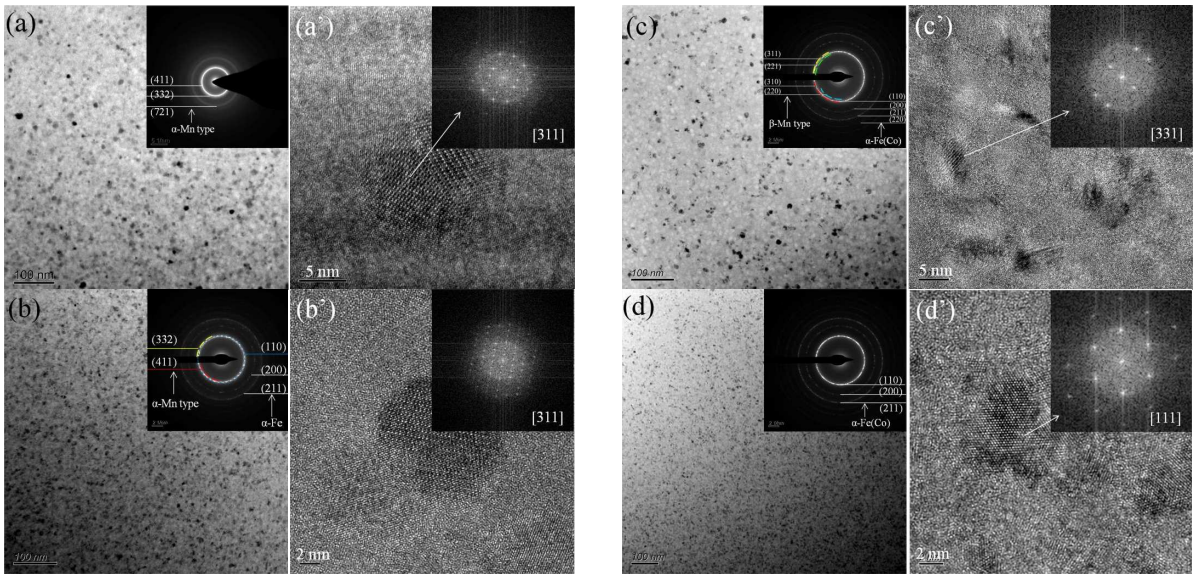


Fig. 4. TEM images, SAED patterns, HRTEM images, and FFTs patterns of the four kinds of alloys annealed at 848 K: (a), (a′) $Fe_{72}Nb_{12}B_{16}$, (b), (b′) $Fe_{72}Nb_{12}B_{15}Cu_1$, (c), (c′) $Fe_{36}Co_{36}Nb_{12}B_{16}$, and (d), (d′) $Fe_{36}Co_{36}Nb_{12}B_{15}Cu_1$.

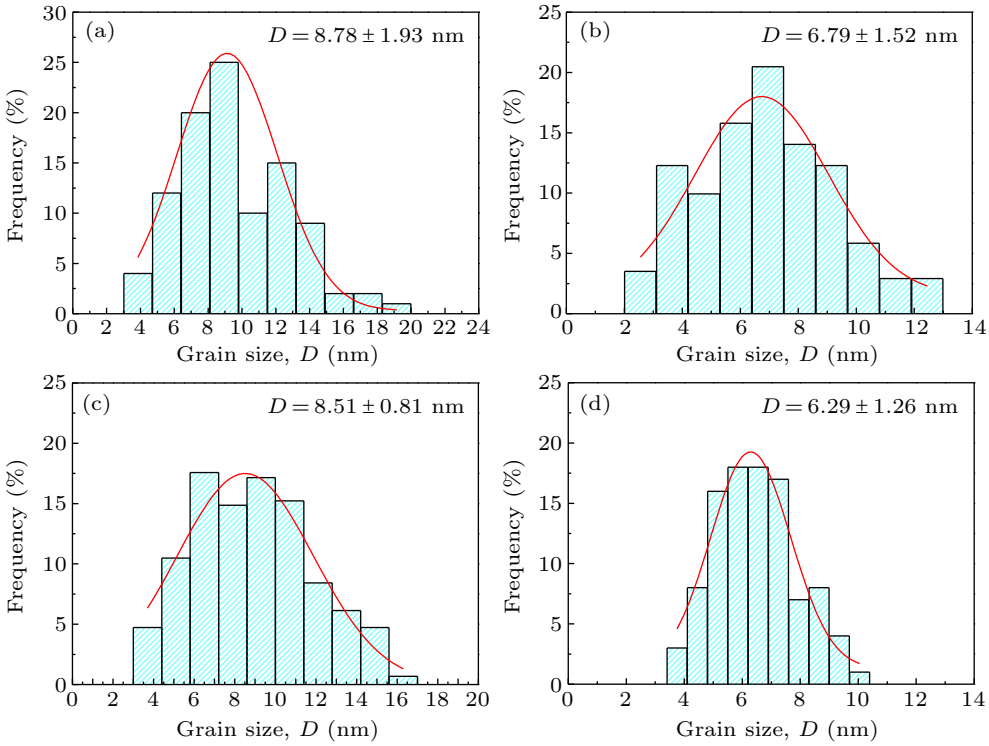


Fig. 5. Grain size distributions of (a) $Fe_{72}Nb_{12}B_{16}$, (b)$Fe_{72}Nb_{12}B_{15}Cu_1$, (c) $Fe_{36}Co_{36}Nb_{12}B_{16}$, and (d) $Fe_{36}Co_{36}Nb_{12}B_{15}Cu_1$ alloys annealed at 848 K.

Both XRD and TEM show that the primary crystallization phase of $Fe_{72}Nb_{12}B_{16}$ is an α-Mn-type metastable phase. The addition of 1 at.% Cu mostly changes the initial crystallization phase of the alloy. Cu is insoluble in α-Fe nanocrystals and serves as a heterogeneous nucleation site in Nanoperm.[34] In this study, Cu addition decreases the volume fraction of the α-Mn-type metastable phase during crystallization. However, the addition of 1 at.% Cu cannot completely inhibit the precipitation of the metastable phase. When adding 36 at.% Co, the addition of Co has a significant influence on the crystallization because the mixing enthalpy of Co–Nb (-25 kJ/mol) is larger than that of Fe–Nb (-16 kJ/mol).[35] Co addition results in the redistribution of Nb and affects the crystallization behaviors. Moreover, Cu clusters serve as heterogeneous nucleation sites for the formation of α-Fe(Co) form when the $Fe_{36}Co_{36}Nb_{12}B_{15}Cu_1$ alloy is annealed at 848 K.

Coercivity (H_c) values of the $Fe_{72}Nb_{12}B_{16}$, $Fe_{72}Nb_{12}B_{15}Cu_1$, $Fe_{36}Co_{36}Nb_{12}B_{16}$, and $Fe_{36}Co_{36}Nb_{12}B_{15}Cu_1$ alloys depend on the annealing temperature (T_a, Fig. 7). Because of the different crystallization behaviors of the four kinds of alloys, the change in H_c values with annealing temperature also varies.

For the $Fe_{72}Nb_{12}B_{16}$ alloy, H_c has little change below 848 K and continuously increases with the increase of annealing temperature. Both H_c of $Fe_{36}Co_{36}Nb_{12}B_{16}$ and $Fe_{72}Nb_{12}B_{16}Cu_1$ alloys increase initially, decrease, and ultimately increase with increasing annealing temperature. At the initial stage of crystallization, heat treatment of the amorphous alloys can reduce the internal stress produced during their preparation, thus reducing the H_c value of the alloy. However, H_c of $Fe_{72}Nb_{12}B_{16}$, $Fe_{72}Nb_{12}B_{15}Cu_1$, and $Fe_{36}Co_{36}Nb_{12}B_{16}$ alloys annealed at 823 K does not decrease. The large H_c values at the beginning of crystallization are owing to the formation of the metastable phase. Later, the decrease of H_c of $Fe_{72}Nb_{12}B_{15}Cu_1$ and $Fe_{36}Co_{36}Nb_{12}B_{16}$ alloys is due to the disappearance of the metastable phase. At 973 K, H_c values of the $Fe_{72}Nb_{12}B_{15}Cu_1$, $Fe_{36}Co_{36}Nb_{12}B_{16}$, and $Fe_{36}Co_{36}Nb_{12}B_{15}Cu_1$ alloys are similar. In the whole annealing temperature range, $Fe_{72}Nb_{12}B_{16}$ and $Fe_{36}Co_{36}Nb_{12}B_{16}$ possess relatively high H_c. Both large H_c values in the early stage of crystallization are attributed to the metastable phase. The content of the β-Mn-type metastable phase is significantly greater than that of the α-Mn-type metastable phase. However, the H_c of $Fe_{36}Co_{36}Nb_{12}B_{16}$ alloy is greater than that of $Fe_{72}Nb_{12}B_{16}$ alloy. It should be that the β-Mn-type metastable phase has a greater magnetocrystalline anisotropy. At 973 K, the H_c of $Fe_{72}Nb_{12}B_{16}$ alloy is greater than that of other alloys. This is attributed to the larger grain size of the α-Fe phase. Below 973 K, the H_c values of the $Fe_{36}Co_{36}Nb_{12}B_{15}Cu_1$ alloy are lower than those of other alloys. For the $Fe_{36}Co_{36}Nb_{12}B_{15}Cu_1$ alloy, the low H_c value is related to the formation of a dual-phase [amorphous + α-Fe(Co) nanocrystalline] structure. For the dual-phase alloys, when the grain size (D) of the nanocrystalline is smaller than the ferromagnetic exchange interaction length,[36] magnetocrystalline anisotropy is effectively evened out and H_c obeys a D^6 power law. The H_c is also related to the uniformity of grain distribution. According to Figs. 4(d) and 5(d), the distribution of the nanograins is uni-

form and the mean grain size is fine. Therefore, the H_c of the $Fe_{36}Co_{36}Nb_{12}B_{15}Cu_1$ alloy is lowest at the initial stage of crystallization. D of the $Fe_{36}Co_{36}Nb_{12}B_{15}Cu_1$ alloy increases with the increase of annealing temperature. Therefore, the H_c value of the $Fe_{36}Co_{36}Nb_{12}B_{15}Cu_1$ alloy increases gradually above 848 K. At 1023 K, the precipitation of numerous intermetallic compounds leads to the rapid increase in H_c for the four kinds of alloys.

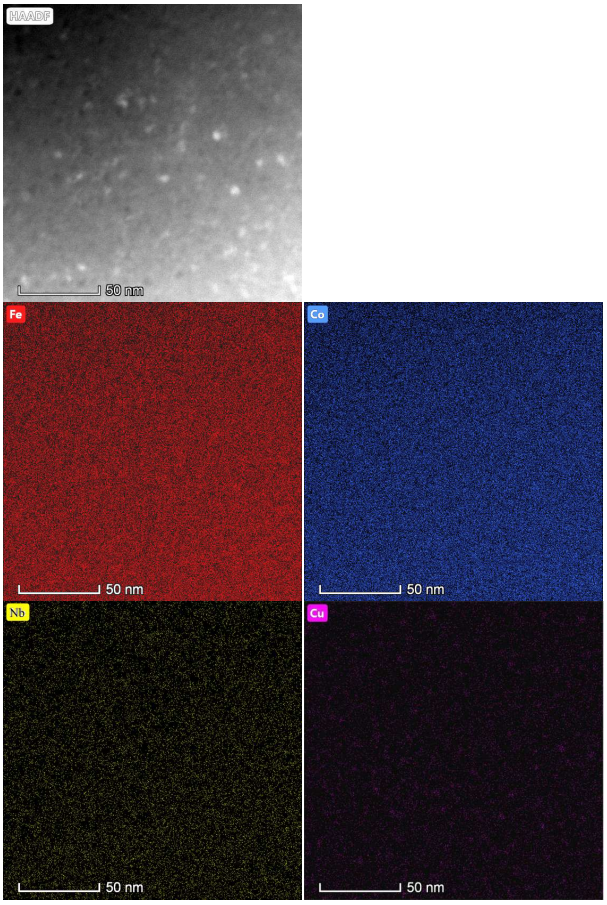


Fig. 6. TEM image and the corresponding EDS elemental maps of the $Fe_{36}Co_{36}Nb_{12}B_{15}Cu_1$ alloy annealed at 848 K.

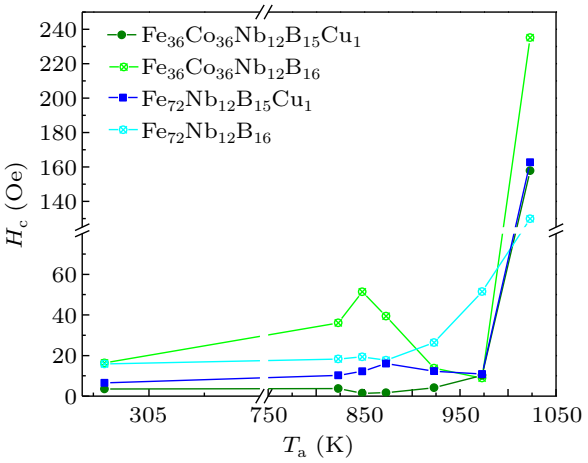


Fig. 7. Dependence of H_c of $Fe_{72}Nb_{12}B_{16}$, $Fe_{72}Nb_{12}B_{15}Cu_1$, $Fe_{36}Co_{36}Nb_{12}B_{16}$, and $Fe_{36}Co_{36}Nb_{12}B_{15}Cu_1$ alloys on annealing temperature (T_a).

4. Conclusion

Four kinds of amorphous and nanocrystalline alloys, $Fe_{72}Nb_{12}B_{16}$, $Fe_{72}Nb_{12}B_{15}Cu_1$, $Fe_{36}Co_{36}Nb_{12}B_{16}$, and $Fe_{36}Co_{36}Nb_{12}B_{15}Cu_1$, were prepared. The effects of Cu and Co addition alone and those of Cu and Co addition in combination on the crystallization and magnetic properties of the $Fe_{72}Nb_{12}B_{16}$ alloy were investigated.

(i) The four kinds of alloys have different crystallization behaviors. The primary crystallization phases are notably different. Metastable phases are observed for the $Fe_{72}Nb_{12}B_{16}$, $Fe_{72}Nb_{12}B_{15}Cu_1$, and $Fe_{36}Co_{36}Nb_{12}B_{16}$ alloys. The primary crystallization phase of the $Fe_{36}Co_{36}Nb_{12}B_{15}Cu_1$ alloy with both Cu and Co additions is the α-Fe(Co) crystalline phase.

(ii) At the initial stage of crystallization, for the $Fe_{72}Nb_{12}B_{16}$ alloy, the addition of 1 at.% Cu decreases the grain size of the crystals, and the addition of 36 at.% Co has little impact. The grain size of the $Fe_{36}Co_{36}Nb_{12}B_{15}Cu_1$ alloy is markedly refined when both Cu and Co are added. The EDS elemental maps show that Cu clustering occurs. The SAED analysis and HRTEM image further indicate that the co-addition of Cu and Co completely inhibits the precipitation of the metastable primary phase.

(iii) Compared with other alloys, $Fe_{36}Co_{36}Nb_{12}B_{15}Cu_1$ alloy exhibits a lower H_c below 973 K. The co-addition of Cu and Co decreases H_c on the whole.

Acknowledgments

Project supported by the National Natural Science Foundation of China (Grant No. 21905110), the Natural Science Foundation of Jilin Province of China (Grant No. YDZJ202201ZYTS319), and the Sinoma Institute of Materials Research Co., Ltd. of Guangzhou Province of China.

References

[1] Zhang J H, Zhang C Z, Zhang X X, Li Z E, He A N, Song J C and Chang C T 2021 *J. Alloys Compd.* **866** 158991
[2] Ohta M and Chiwata N 2020 *J. Magn. Magn. Mater.* **509** 166838
[3] Xie L, Wang A D, Yue S Q, He A N, Chang C T, Li Q, Wang X M and Liu C T 2019 *J. Magn. Magn. Mater.* **483** 158
[4] Liu T, Li F C, Wang A D, Xie L, He Q F, Luan J H, He A N, Wang X M, Liu C T and Yang Y 2019 *J. Alloys Compd.* **776** 606
[5] Ri M C, Ding D W, Sun Y H and Wang W H 2021 *J. Mater. Sci. Technol.* **69** 1
[6] Sun Y M, Wang Z Q, Xu S C and Hua Z 2021 *Chin. Phys. B* **30** 038103
[7] Lyasotsky I V, Dyakonova N B and Dyakonov D L 2014 *J. Alloys Compd.* **586** S20
[8] Yoshizawa Y, Oguma S and Yamauchi K 1988 *J. Appl. Phys.* **64** 6044
[9] Suzuki K, Makino A, Kataoka N, Inoue A and Masumoto T 1991 *Mater. Trans., JIM* **32** 93
[10] Willard M A, Laughlin D E, McHenry M E, Thoma D, Sickafus K, Cross J O and Harris V G 1998 *J. Appl. Phys.* **84** 6773
[11] Makino A, Men H, Kubota T, Yubuta K and Inoue A 2009 *IEEE Trans. Magn.* **45** 4302
[12] Liu T, Kong F Y, Xie L, Wang A D, Chang C T, Wang X M and Liu C T 2017 *J. Magn. Magn. Mater.* **441** 174
[13] Jiang T H, Zhao M, Xiang Q C, Ren Y L, Li Q F and Qiu K Q 2020 *AIP Adv.* **10** 105123
[14] Jha R, Diercks D R, Chakraborti N, Stebner A P and Ciobanu C V 2019 *Scripta Mater.* **162** 331

[15] Yu W Q, Lin H, Lu L P, Wang L and Xing G Z 2020 *Phys. Lett. A* **384** 126640

[16] Yoon S and Lee S J 2014 *Mater. Trans.* **55** 1517

[17] Kong F L, Men H, Zhang M X, Liu T C, Xie G Q and Shen B L 2012 *Appl. Phys. A* **108** 211

[18] Ohkubo T, Kai H, Ping D H, Hono K and Hirotsu Y 2001 *Scripta Mater.* **44** 971

[19] Hono K, Ping D H, Ohnuma M and Onodera H 1999 *Acta Mater.* **47** 997

[20] Ping D H, Wu Y Q, Hono K, Willard M A, Mchenry M E and Laughlin D E 2001 *Scripta Mater.* **45** 781

[21] He A N, Li J W, Wang M K, Wang A D, Xiao Y, Dong Y Q, Guo H, Jiang R R, Xia W X, Dong L H, Wang H D and Ge J Y 2022 *J. Mater. Sci. Technol.* **120** 1

[22] Yu W Q, Lu L P, Zuo B, Hua Z, Xing G L, Wang X Y and Wang D D 2019 *Appl. Phys. A* **125** 636

[23] Xiang R, Zhou S X, Dong B S, Zhang G Q, Li Z Z, Wang Y G and Chang C T 2014 *Prog. Nat. Sci.* **24** 649

[24] Xue L, Yang W M, Liu H S, Men H, Wang A D, Chang C T and Shen B L 2016 *J. Magn. Magn. Mater.* **419** 198

[25] Zuo B, Yu X, Wang X N and Wang Z Q 2019 *Met. Sci. Heat Treat.* **61** 23

[26] Xiong X Y, Muddle B C and Finlayson T R 2003 *J. Phys. D: Appl. Phys.* **36** 223

[27] Takeshi N and Yukichi U 2006 *ISIJ Int.* **46** 1371

[28] Sun Y M, Yu W Q, Long D, Zhang Y and Hua Z 2015 *Mod. Phys. Lett. B* **29** 1550196

[29] Imafuku M, Sato S, Koshiba H, Matsubara E and Inoue A 2001 *Scripta Mater.* **44** 2369

[30] Dyakonova N B, Dyakonov D L and Lyasotskyi I V 2014 *J. Alloys Compd.* **586** S41

[31] Zamiri R, Hamid-Reza B, Zakaria A, Jorfi R, Zamiri G, Rebelo A and Omar A A 2013 *Chin. Phys. Lett.* **30** 118103

[32] Jiang M Y, Zhu Z J, Chen C K, Li X and Hu X J 2019 *Acta Phys. Sin.* **68** 148101 (in Chinese)

[33] Pradeep K G, Herzer G, Choi P and Raabe D 2014 *Acta Mater.* **68** 295

[34] Blázquez J S, Franco V and Conde A 2002 *J. Phys.: Condens. Matter* **14** 11717

[35] Takeuchi A and Inoue A 2005 *Mater. Trans.* **46** 2817

[36] Suzuki K, Ito N, Garitaonandia J S, Cashion J D and Herzer G 2008 *J. Non-Cryst. Solids* **354** 5089